

LETTER TO THE EDITOR

Is the overconcentration of pristine populations in Galactic globular clusters real?

An N -body approach to the problem.

P. Berczik^{2,3,1}, O. Sobodar^{1,2}, F. Flammini Dotti^{4,5,6}, M. Sobolenko^{1,2}, M. Ishchenko^{1,2,3}, R. Spurzem^{7,8,9},
M. Giersz², and A. Askar²

¹ Main Astronomical Observatory, National Academy of Sciences of Ukraine, 27 Akademika Zabolotnoho St, 03143 Kyiv, Ukraine
e-mail: berczik@mao.kiev.ua

² Nicolaus Copernicus Astronomical Centre, Polish Academy of Sciences, ul. Bartycka 18, 00-716 Warsaw, Poland

³ Fesenkov Astrophysical Institute, Observatory 23, 050020 Almaty, Kazakhstan

⁴ Department of Physics, New York University Abu Dhabi, PO Box 129188 Abu Dhabi, UAE

⁵ Center for Astrophysics and Space Science (CASS), New York University Abu Dhabi, PO Box 129188, Abu Dhabi, UAE

⁶ Dipartimento di Fisica, Sapienza, Università di Roma, P.le Aldo Moro, 5, 00185 - Rome, Italy

⁷ National Astronomical Observatories, Chinese Academy of Sciences, 20A Datun Rd., Chaoyang District, 100101, Beijing, China

⁸ Kavli Institute for Astronomy and Astrophysics, Peking University, 5 Yi He Yuan Road, Haidian District, Beijing 100871, P.R. China

⁹ Astronomisches Rechen-Institut, Zentrum für Astronomie der Universität Heidelberg, Mönchhofstraße 12-14, D-69120 Heidelberg, Germany

February 19, 2026

ABSTRACT

Aims. Recent observations indicate that in some Milky Way globular clusters (GCs) pristine red giant branch (RGB) stars appear more centrally concentrated than enriched ones. This contradicts most multiple stellar population (MSP) formation scenarios, which predict that the enriched (second) population (2P) should initially be more concentrated than the pristine (first) population (1P). Previous MOCCA Monte Carlo simulations suggested that this apparent overconcentration is a transient effect arising in clusters that have lost a large fraction of their initial mass and host an active black hole subsystem (BHS), and is visible only when RGB stars are used as tracers. In this letter, we test this interpretation using tailored NBODY6++GPU models evolved with direct N -body simulations, providing an independent validation that does not rely on a statistical treatment of relaxation.

Methods. We performed direct N -body simulations with the NBODY6++GPU code, adopting initial conditions designed to reproduce the dynamical regime relevant to the proposed mechanism. The simulations include updated stellar and binary evolution, dynamical interactions, and the Galactic tidal field, enabling a direct comparison with MOCCA results.

Results. The simulations confirm that the spatial distributions and kinematics inferred from RGB stars can be strongly affected by stochastic fluctuations and interactions with the BHS. Preferential ejection of 2P RGB and their progenitors from the cluster centre leads to a transient apparent overconcentration of 1P RGB stars, in agreement with earlier MOCCA predictions. We show that this effect does not reflect the global MSP structure and that analyses based solely on RGB tracers may yield biased interpretations. These results support the view that dynamical evolution within current MSP formation scenarios can account for the apparent 1P overconcentration inferred in clusters such as NGC 3201 and NGC 6101.

Key words. stellar dynamics – methods: numerical – globular clusters: evolution – stars: multiple stellar populations

1. Introduction

Globular clusters (GCs) are among the simplest stellar systems and have long been regarded as nearly spherical and chemically homogeneous. However, photometric and spectroscopic studies have revealed the presence of multiple stellar populations (MSP), characterised by variations in light-element abundances (see [Bastian & Lardo 2018](#); [Gratton et al. 2019](#), and references therein). The pristine population (1P) has a chemical composition similar to field stars of comparable metallicity, while the second population (2P) is enriched in light elements. The fraction of 2P stars in Milky Way GCs correlates strongly with GC mass, increasing from $\sim 40\%$ in low-mass systems to $\sim 90\%$ in the most massive clusters ([Milone & Marino 2022](#)).

Despite extensive efforts, the formation and evolution of MSPs remain uncertain. Most scenarios predict that 2P forms more centrally concentrated than 1P and gradually mixes with it through dynamical evolution (e.g. [Bastian & Lardo 2018](#)). Observational studies largely support this expectation and have characterised spatial and kinematic differences between sub-populations in increasing detail (e.g. [Kamann et al. 2020a,b](#); [Libralato et al. 2023](#); [Dalessandro et al. 2024](#); [Leitinger et al. 2025](#); [Cordoni et al. 2025](#)).

Recently, however, [Leitinger et al. \(2023\)](#) reported that in NGC 3201 and NGC 6101 the 1P inferred from red giant branch (RGB) stars appears more centrally concentrated than 2P, challenging standard MSP scenarios. Subsequent work has shown that the interpretation of radial trends can depend sensitively on

methodology and tracer selection. In particular, [Cadelano et al. \(2024\)](#) demonstrated that in NGC 3201 the enriched population remains more centrally concentrated within $\sim 1.5 r_h$ and exhibits a bimodal radial structure not captured by cumulative diagnostics, while [Mehta et al. \(2025\)](#) independently confirmed the central concentration of enriched stars using Gaia XP spectrophotometry. These results highlight the complexity of MSP radial structure and the importance of complementary diagnostics.

Motivated by these developments, [Giersz et al. \(2025b\)](#), used MOCCA simulations within the asymptotic giant branch (AGB) ejecta enrichment framework in which 2P stars form centrally from gas polluted by the processed ejecta of AGB stars. The authors proposed that the apparent inversion seen in cumulative RGB-based diagnostics may be a transient effect caused by small-number statistics and enhanced dynamical interactions with a black hole subsystem (BHS), particularly affecting initially concentrated 2P stars. In this interpretation, the effect is tracer-population dependent and does not reflect the global MSP structure.

Here we test this scenario using direct N -body simulations with the NBODY6++GPU code. As MOCCA relies on a statistical solution of the Fokker–Planck equations, independent verification with direct N -body methods provides a complementary assessment of the proposed mechanism. By modelling clusters in the relevant dynamical regime, we examine whether the transient RGB-based inversion arises without Monte Carlo approximations. The paper is organised as follows. In Sect. 2 we describe the NBODY6++GPU and MOCCA codes and outline the adopted initial conditions. In Sect. 3 we present the simulation results. In Sect. 4 we summarise and discuss our findings.

2. Method and initial conditions

2.1. The MOCCA and NBODY6++GPU code

In this work, we performed numerical simulations using the MOCCA Monte Carlo code ([Giersz 1998](#); [Hypki & Giersz 2013](#); [Giersz et al. 2013](#); [Hypki et al. 2022, 2025](#); [Giersz et al. 2025a](#)) and the direct N -body code NBODY6++GPU ([Spurzem & Kamlah 2023](#), and references therein). MOCCA is based on Hénon’s Monte Carlo method ([Hénon 1971](#); [Stodkiewicz 1982](#)) and relies on a statistical solution of the Fokker–Planck equations. To model dynamical interactions of small- N subsystems, it employs the FEWBODY package ([Fregeau et al. 2004](#); [Fregeau & Rasio 2007](#)). MOCCA performs full stellar and dynamical evolution of realistic-size GCs up to a Hubble time.

NBODY6++GPU is a direct N -body code optimised for studying the dynamical evolution of star clusters and galaxies. It integrates large- N systems using GPU acceleration and parallelisation across multiple GPU cores ([Nitadori & Aarseth 2012](#); [Wang et al. 2015](#); [Huang et al. 2016](#)). Recent developments of direct N -body frameworks for modelling composite stellar populations include NbodyCP ([Li & Spurzem 2026](#)), highlighting the growing capability of direct N -body codes to treat MSPs self-consistently. Hard binaries are handled using Kustaanheimo–Stiefel (KS) regularisation ([Kustaanheimo & Stiefel 1965](#)).

Both MOCCA and NBODY6++GPU use consistent prescriptions for single and binary stellar evolution, stellar winds, supernova kicks, and gravitational recoil from black hole mergers, with the most recent updates described in [Kamlah et al. \(2022a\)](#); [Giersz et al. \(2025a\)](#). The MOCCA code has been extensively tested against direct N -body simulations, including NBODY6++GPU, and shows very good agreement across

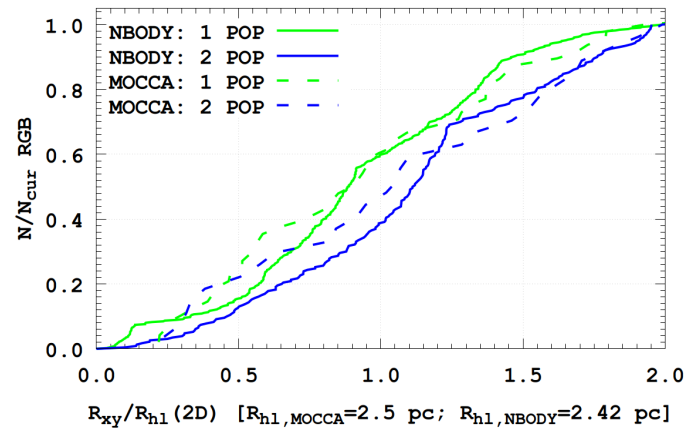


Fig. 1. Cumulative number distributions of RGB stars for 1P (green) and 2P (blue) around 1.2 Gyr as a function of projected distance, normalised by the 2D half-light radius R_{hl} . Solid line: N -body model (average of 33 snapshots). Dashed line: MOCCA model (average of 5 snapshots). Snapshots span 1.18–1.22 Gyr.

a wide range of cluster environments (e.g. [Giersz et al. 2008](#); [Wang et al. 2016](#); [Madrid et al. 2017](#); [Geller et al. 2019](#); [Rizzuto et al. 2021](#); [Kamlah et al. 2022b](#); [Vergara et al. 2025](#)).

2.2. Initial conditions

The initial conditions of the N -body model were chosen carefully, as large-scale direct N -body simulations are computationally expensive and time-consuming. Reproducing the cluster model presented in [Giersz et al. \(2025b\)](#) would require months of computation, mainly because of its very high primordial binary fraction ($f_b = 0.95$) and the non-parallelised treatment of internal binary evolution ([Huang et al. 2016](#)). We therefore focused on reproducing the findings of [Giersz et al. \(2025b\)](#), namely the apparent 1P overconcentration in clusters close to dissolution, characterised by a small number of RGB stars and the presence of an active BHS. The selected N -body model dissolves on a much shorter timescale than a typical Milky Way GC, but it captures the essential physical processes relevant to the proposed mechanism.

The adopted initial conditions are as follows: initial number of particles $N_{1\text{P}} = 61\,000$ and $N_{2\text{P}} = 30\,500$, with a [Kroupa \(2001\)](#) initial mass function (IMF). The 1P stars were sampled in the mass range $0.08\text{--}150\,\text{M}_\odot$, while the 2P stars were sampled between 0.08 and $20\,\text{M}_\odot$. Both populations have metallicity $Z_{1\text{P}} = 0.001$ and $Z_{2\text{P}} = 0.001$, with binary fractions $f_{b,1\text{P}} = 0.1$ and $f_{b,2\text{P}} = 0.1$.

These parameters correspond to an initial cluster mass of $M(0) = 56\,953.8\,\text{M}_\odot$. The cluster is placed at a Galactocentric distance of $R_G = 2\,\text{kpc}$ in a point-mass Galactic potential with $M_G = 2.25 \times 10^{10}\,\text{M}_\odot$. The ratio of half-mass radii is $R_{h,2\text{P}}/R_{h,1\text{P}} = 0.1$. The two populations are initially in virial equilibrium, with the 1P component slightly tidally underfilling ($R_{\text{tid}} = 18.9\,\text{pc}$). The initial King model ([King 1966](#)) concentration parameters are $W_0 = 3.0$ for 1P and $W_0 = 7.0$ for 2P. The initial conditions were generated using the publicly available McLuster¹ code ([Küpper et al. 2011](#); [Leveque et al. 2022](#)).

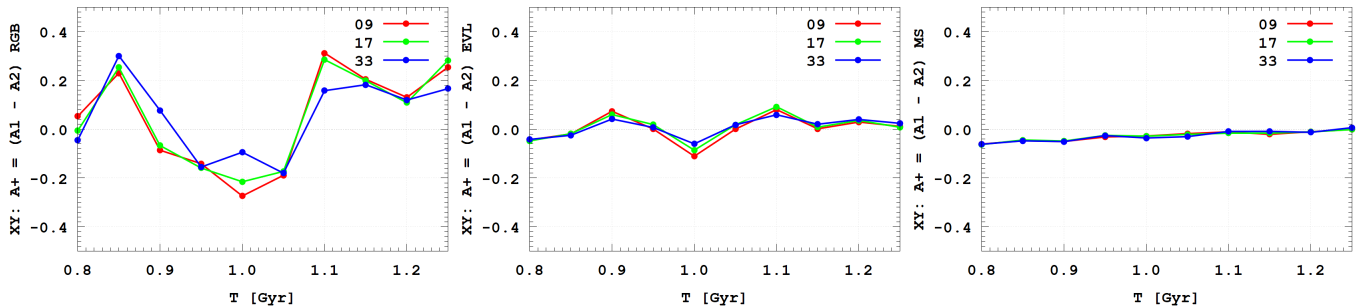


Fig. 2. The time evolution of the A^+ parameter for different type of stars and for $X - Y$ projection of 3D snapshots. The left panel shows RGB stars, the middle panel – evolved luminous stars and the right panel – MS stars. The red, green and blue lines are averaged over 9, 17 and 33 snapshots, respectively.

3. Results

Following the approach presented in (Leitinger et al. 2023), we used the A^+ parameter (Alessandrini et al. 2016; Dalessandro et al. 2018, 2019) to assess the degree of spatial mixing between 1P and 2P. As an illustration of the A^+ parameter calculation, we show in Fig. 1 the cumulative projected distributions of RGB stars for both stellar populations of N -body and MOCCA simulations, respectively. Both distributions are normalised by their masses and their respective half-light radii. The total number of RGB stars at the reference time 1.2 Gyr is quite small, $N_{\text{RGB}} = 22$ (see Fig. A.1 in the Appendix), so we decided to collect data from snapshots between 1.18 – 1.22 Gyr to improve the statistics and plot the averaged mass distribution at 1.2 Gyr. The MOCCA model has 5 snapshots, while the N -body model has 33 snapshots. Figure 1 shows that the number of RGB stars per snapshot is consistent and does not depend on the number of snapshots included in the average. The time steps for snapshots are 0.116 Myr and 10 Myr for NBODY6++GPU and MOCCA simulations, respectively.

Figure 1 shows that both models predict the 1P RGB population to be more centrally concentrated than the 2P RGB population. Taking into account that we are comparing two simulations done with two different codes, the agreement between the 2D projected mass distributions of RGB stars for both models is very good. Small differences in the curves reflect the stochastic spatial distribution of the small RGB sample and the different time averaging of snapshots, since MOCCA averages over a longer interval than the N -body results; therefore identical shapes are not expected. The A^+ parameters are 0.15 and 0.12 for NBODY6++GPU and MOCCA models, respectively, at 1.2 Gyr.

The time evolution of the A^+ parameter for different types of stars and for $X - Y$ projection (in the Galactic coordinate system) of 3D snapshots is presented in Fig. 2. The time range shown in the figure is from 0.8 to 1.25 Gyr. On the three panels, we show the time evolution for the different types of stars: RGB stars, evolved luminous stars and main sequence (MS) stars. Each line presented in the figures is calculated by averaging a different number of snapshots. Each curve is computed using a sliding average over a window of snapshots centred on the reference time: 9 (± 4), 17 (± 8), or 33 (± 16) snapshots. The red, green, and blue curves correspond to these three averaging windows, respectively.

Generally, every three averages gives a more or less consistent result for MS stars (right panel) and other types of luminous stars (middle panel). For the most interesting case of RGB stars (left panel), the snapshot averaging gives slightly different re-

sults depending on the time, with a spread of at most about 0.1. The spread is much smaller than the variation of the A^+ parameter itself. The changes of the sign of the A^+ parameter happen on the timescale of about 0.15 Gyr, indicating strong time variability. On short timescales, 1P becomes overconcentrated relative to 2P and then quickly returns to a less concentrated state. The 1P overconcentration is a transient feature, and it confirms the findings of Giersz et al. (2025b).

The Giersz et al. (2025b) conclusions are further confirmed by the time evolution of the A^+ parameter for MS and luminous evolved stars. They do not show any significant variation in the A^+ parameter and keep values close to 0. Both populations are fully mixed for MS and evolved luminous stars. Further confirmation of the transient feature of the overconcentration of 1P RGB population over the 2P RGB population is provided by Fig. A.2 in the Appendix, in which the evolution of the A^+ parameter for different projections of the 3D snapshots is presented, namely: $X - Y$, $X - Z$ and $Y - Z$ projections. We see that the A^+ parameter shows similar strong variations and transient character for all projections. The transient overconcentration of 1P RGB stars is not driven by projection effects, but instead reflects the time evolution of the spatial distributions of RGB stars in the 1P and 2P populations.

4. Conclusions

We confirm the results of Giersz et al. (2025b), showing that when the analysis is based on RGB stars, the 1P population can appear more centrally concentrated than 2P at radii of a few half-light radii. Using direct N -body simulations tailored to reproduce the dynamical regime relevant to the proposed mechanism, we demonstrate that this apparent inversion is a transient feature and depends strongly on the adopted stellar tracers.

This effect is particularly relevant for GCs with present-day masses of a few $10^5 M_\odot$, which have retained only $\sim 10\%$ of their initial mass and host an active BHS. In such systems, small-number statistics and strong dynamical interactions can significantly influence the spatial distribution of RGB stars, potentially leading to biased inferences about the global MSP structure when observations are restricted to this tracer population. To capture these processes while maintaining feasible computational cost, we adopted a reduced- N model with an accelerated evolutionary timescale. Despite these simplifications, the simulations reproduce the key evolutionary behaviour of the reference MOCCA model.

Figure 2 shows that the A^+ parameter derived from RGB stars varies strongly over time, ranging between -0.3 and 0.4 over ~ 0.45 Gyr. In contrast, for evolved luminous stars (ex-

¹ <https://github.com/agostinolev/mcluster>

cluding compact remnants), A^+ remains close to zero, indicating near-complete mixing of the populations. When computed using only MS stars, the evolution follows the expected monotonic trend toward spatial mixing. The MOCCA simulation exhibits a comparable transient signal near 1.2 Gyr, with $A^+ \simeq 0.12$, in close agreement with the NBODY6++GPU result ($A^+ \simeq 0.15$), providing independent validation of the Monte Carlo interpretation.

Consistent with the scenario proposed by [Giersz et al. \(2025b\)](#), the simulated cluster hosts an active BHS and is close to dissolution. At this stage, BHs contribute $\sim 8\%$ of the cluster mass while the cluster retains only $\sim 10\%$ of its initial mass. The RGB population is correspondingly sparse, placing the system in a regime where stochastic spatial fluctuations and enhanced interactions between the BHS and centrally concentrated 2P progenitors amplify transient segregation signatures.

A similar role of dynamical interactions in removing centrally concentrated 2P stars from the cluster centre has recently been identified by [Pavlík et al. \(2025\)](#), who investigated spatial mixing driven by binary-single scattering with direct N -body simulations. Although their models do not show an inversion of the cumulative profiles, enriched stars are preferentially scattered to larger radii through binary-single encounters. The absence of inversion likely reflects the lack of strong mass loss and near-dissolution evolution in their clusters. Taken together, these results suggest that while dynamical scattering can significantly modify MSP radial structure, the emergence of an apparent inversion requires clusters to have lost a substantial fraction of their initial mass.

Projection-dependent variations in the inferred A^+ evolution further demonstrate the sensitivity of cumulative diagnostics to sampling effects and viewing geometry. While these fluctuations do not alter the qualitative conclusion regarding the transient nature of RGB-based segregation, they highlight the importance of using multiple complementary diagnostics when interpreting spatial distributions. This is particularly relevant in light of recent observational work showing complex and sometimes non-monotonic radial behaviour of MSPs (e.g. [Cadelano et al. 2024](#); [Mehta et al. 2025](#)), where cumulative metrics alone may not fully capture underlying structural features.

Our results therefore do not imply that enriched populations are globally less concentrated than pristine ones, but rather that tracer selection and dynamical state can produce apparent inversions in specific diagnostics. In this context, the transient behaviour identified here may provide a dynamical pathway contributing to the observational diversity reported in recent studies.

We conclude that analyses based solely on RGB tracers should be interpreted with caution, and that complementary approaches using larger and dynamically less biased samples, such as MS stars, are essential for robust inference of MSP structure. Further observational tests of tracer-dependent segregation and comparisons with diagnostics beyond cumulative distributions would provide valuable constraints on MSP formation scenarios, including the AGB framework and alternatives.

Acknowledgements. PB, MI, MS and OS thank the support from the special program of the Polish Academy of Sciences and the U.S. National Academy of Sciences under the Long-term program to support Ukrainian research teams, grant No. PAN.BFB.S.BWZ.329.022.2023. This material is based upon work supported by Tamkeen under the NYU Abu Dhabi Research Institute grant CASS. PB and MI thank Project No. BR24992759 “Development of the concept for the first Kazakhstani orbital cislunar telescope - Phase I”, financed by the Ministry of Science and Higher Education of the Republic of Kazakhstan. RS acknowledges NAOC International Cooperation Office for its support in 2023, 2024, and 2025. RS acknowledges Chinese Academy of Sciences President’s International Fellowship Initiative for Visiting Scientists (PIFI, grant No. 2026PVA0089), and the National Natural Science Foundation of China (NSFC) under grant No. 12473017. This research was supported in part by the grant NSF PHY-2309135

to the Kavli Institute for Theoretical Physics (KITP). RS and FFD acknowledge German Science Foundation (DFG) grant Sp 345/24-1. MG was supported by the Polish National Science Center (NCN) through the grant 2021/41/B/ST9/01191. AA acknowledges that this research was funded in part by National Science Centre (NCN), Poland, grant No. 2024/55/D/ST9/02585. For the purpose of Open Access, the author has applied a CC BY public copyright licence to any Author Accepted Manuscript (AAM) version arising from this submission.

Data Availability

The data for the MOCCA and NBODY6++GPU model described in this paper, including the data for RGB star distribution, is available at <https://zenodo.org/records/temp>. Additional data can be provided upon request to the corresponding authors.

References

Alessandrini, E., Lanzoni, B., Ferraro, F. R., Miocchi, P., & Vesperini, E. 2016, *ApJ*, 833, 252

Bastian, N. & Lardo, C. 2018, *ARA&A*, 56, 83

Cadelano, M., Dalessandro, E., & Vesperini, E. 2024, *A&A*, 685, A158

Cordoni, G., Casagrande, L., Milone, A. P., et al. 2025, *MNRAS*, 537, 2342

Dalessandro, E., Cadelano, M., Della Croce, A., et al. 2024, *A&A*, 691, A94

Dalessandro, E., Cadelano, M., Vesperini, E., et al. 2019, *ApJ*, 884, L24

Dalessandro, E., Cadelano, M., Vesperini, E., et al. 2018, *ApJ*, 859, 15

Fregeau, J. M., Cheung, P., Portegies Zwart, S. F., & Rasio, F. A. 2004, *MNRAS*, 352, 1

Fregeau, J. M. & Rasio, F. A. 2007, *ApJ*, 658, 1047

Geller, A. M., Leigh, N. W. C., Giersz, M., Kremer, K., & Rasio, F. A. 2019, *ApJ*, 872, 165

Giersz, M. 1998, *MNRAS*, 298, 1239

Giersz, M., Askar, A., Hypki, A., et al. 2025a, *A&A*, 699, A76

Giersz, M., Askar, A., Hypki, A., et al. 2025b, *A&A*, 698, L11

Giersz, M., Heggie, D. C., & Hurley, J. R. 2008, *MNRAS*, 388, 429

Giersz, M., Heggie, D. C., Hurley, J. R., & Hypki, A. 2013, *MNRAS*, 431, 2184

Gratton, R., Bragaglia, A., Carretta, E., et al. 2019, *A&A Rev.*, 27, 8

Hénon, M. H. 1971, *Ap&SS*, 14, 151

Huang, S.-Y., Spurzem, R., & Berczik, P. 2016, *Research in Astronomy and Astrophysics*, 16, 11

Hypki, A. & Giersz, M. 2013, *MNRAS*, 429, 1221

Hypki, A., Giersz, M., Hong, J., et al. 2022, *MNRAS*, 517, 4768

Hypki, A., Vesperini, E., Giersz, M., et al. 2025, *A&A*, 693, A41

Kamann, S., Dalessandro, E., Bastian, N., et al. 2020a, *MNRAS*, 492, 966

Kamann, S., Giesers, B., Bastian, N., et al. 2020b, *A&A*, 635, A65

Kamlah, A. W. H., Leveque, A., Spurzem, R., et al. 2022a, *MNRAS*, 511, 4060

Kamlah, A. W. H., Leveque, A., Spurzem, R., et al. 2022b, *MNRAS*, 511, 4060

King, I. R. 1966, *AJ*, 71, 64

Kroupa, P. 2001, *MNRAS*, 322, 231

Küpper, A. H. W., Maschberger, T., Kroupa, P., & Baumgardt, H. 2011, *MNRAS*, 417, 2300

Kustaanheimo, P. & Stiefel, E. 1965, *Journal fur die reine und angewandte Mathematik*

Leitinger, E., Baumgardt, H., Cabrera-Ziri, I., Hilker, M., & Pancino, E. 2023, *MNRAS*, 520, 1456

Leitinger, E. I., Baumgardt, H., Cabrera-Ziri, I., et al. 2025, *A&A*, 694, A184

Leveque, A., Giersz, M., Banerjee, S., et al. 2022, *MNRAS*, 514, 5739

Li, Z.-M. & Spurzem, R. 2026, *Research in Astronomy and Astrophysics*, 26, 015009

Libralato, M., Vesperini, E., Bellini, A., et al. 2023, *ApJ*, 944, 58

Madrid, J. P., Leigh, N. W. C., Hurley, J. R., & Giersz, M. 2017, *MNRAS*, 470, 1729

Mehta, V. J., Milone, A. P., Casagrande, L., et al. 2025, *MNRAS*, 536, 1077

Milone, A. P. & Marino, A. F. 2022, *Universe*, 8, 359

Nitadori, K. & Aarseth, S. J. 2012, *MNRAS*, 424, 545

Pavlík, V., Davies, M. B., Leitinger, E. I., et al. 2025, *A&A*, 703, A157

Rizzuto, F. P., Naab, T., Spurzem, R., et al. 2021, *MNRAS*, 501, 5257

Spurzem, R. & Kamlah, A. 2023, *Living Reviews in Computational Astrophysics*, 9, 3

Stodólkiewicz, J. S. 1982, *Acta Astron.*, 32, 63

Vergara, M. C., Askar, A., Kamlah, A. W. H., et al. 2025, *arXiv e-prints*, arXiv:2505.07491

Wang, L., Spurzem, R., Aarseth, S., et al. 2016, *MNRAS*, 458, 1450

Wang, L., Spurzem, R., Aarseth, S., et al. 2015, *MNRAS*, 450, 4070

Appendix A: Projection properties of cluster RGB stars

Figure A.1 shows the time evolution of the RGB-star counts in the 1P and 2P populations for projections of the 3D data onto the Galactic coordinate planes ($X - Y$, $X - Z$, and $Y - Z$). The red, green, and blue curves correspond to averages over 9, 17, and 33 snapshots, respectively. For each projection, the lower, middle, and upper curves represent the 2P, 1P, and total population.

As expected, the RGB-star counts in each population are independent of projection direction and therefore show no systematic variation with projection. The larger fluctuations observed in the 2P RGB counts relative to 1P suggest stronger dynamical interactions affecting 2P RGB stars, consistent with the findings of Giersz et al. (2025b).

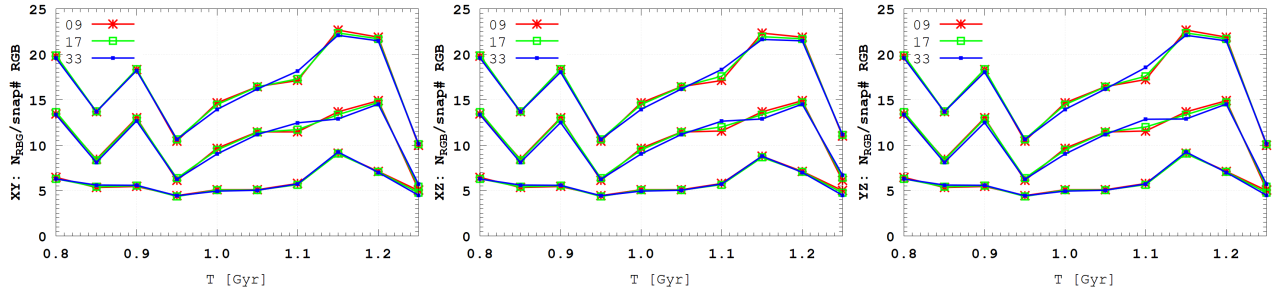


Fig. A.1. Time evolution of the number of RGB stars in the 1P, 2P, and total population for different projections of the 3D snapshots. The left panel shows the $X - Y$ projection, the middle panel the $X - Z$ projection, and the right panel the $Y - Z$ projection. The red, green, and blue lines correspond to averages over 9, 17, and 33 snapshots centred on the selected time, respectively.

In Fig. A.2 we show the evolution of the A^+ parameter for different projections of the 3D snapshots onto the $X - Y$, $X - Z$, and $Y - Z$ planes. The behaviour of A^+ differs between projections, although the amplitude of the fluctuations remains comparable. At 1.2 Gyr, A^+ is positive for the $X - Y$ and $Y - Z$ projections, while it is close to zero for the $X - Z$ projection. This indicates that the inferred spatial distribution of RGB stars depends on the viewing direction.

A weak dependence of A^+ on the number of averaged snapshots is also present. The statistical fluctuations associated with different averaging windows are at the level of $\pm 0.05 - 0.1$, which is significantly smaller than the intrinsic variations of A^+ occurring over time intervals of 0.1–0.15 Gyr. This confirms that the transient behaviour of A^+ reflects genuine changes in the global spatial distribution of RGB stars rather than artefacts of snapshot averaging.

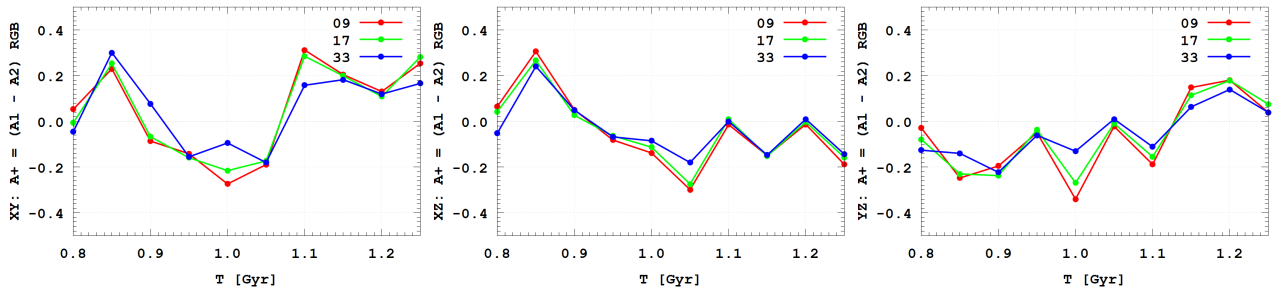


Fig. A.2. Time evolution of the A^+ parameter for RGB stars for projections of the 3D snapshots onto the $X - Y$, $X - Z$, and $Y - Z$ planes (left to right panels). The red, green, and blue lines show averages over 9, 17, and 33 snapshots, respectively.

In Fig. A.3 we show the evolution of the cluster mass normalised to its initial value, together with the ratio of the BHS mass to the current cluster mass. This figure illustrates the key cluster state associated with the transient behaviour of the A^+ parameter. When the cluster mass decreases to ~ 0.1 of its initial value and the BHS mass reaches ~ 0.05 of the current cluster mass, the number of RGB stars becomes very small. In this regime, stochastic fluctuations in their spatial distribution and strong dynamical interactions with the BHS drive the transient variations of A^+ . This behaviour is fully consistent with the findings of Giersz et al. (2025b).

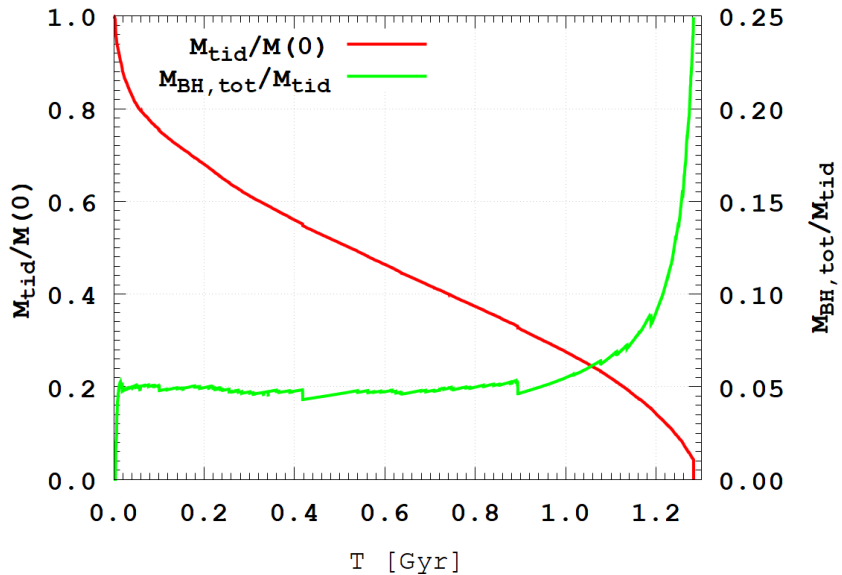


Fig. A.3. NBODY6++GPU evolution of the cluster mass normalised to its initial value $M(0) = 56953.8 \text{ M}_\odot$ (red line) and of the BHS mass normalised to the current cluster mass (green line).